Journal of Chromatography, 609 (1992) 269–276
Elsevier Science Publishers B.V., Amsterdam

CHROM. 24 319

Liquid jet evolution from a gas chromatographic injector

J. Qian*, C. E. Polymeropoulos and R. Ulisse

Department of Mechanical and Aerospace Engineering, Rutgers University, P.O. Box 909, Piscataway, NJ 08855-0909 (USA)

(Received March 6th, 1992)

ABSTRACT

Liquid particles from the breakup of liquid jets produced by a gas chromatographic syringe autoinjection system were observed and measured experimentally. The particle size depended on the motion of the syringe plunger. Very large, fast-moving particles were observed during accelerating periods of the liquid jet. The injection test chamber temperature affected the downstream particle size by heating the liquid before it left the needle and by evaporation into the hot gas. The particles produced by the water and heptane samples used were large and did not lend themselves to rapid vaporization within the gas stream of the gas chromatographic inlet port. Under such conditions, total sample vaporization must be considered either on the hot inlet port wall or on inserts within the inlet port.

INTRODUCTION

A common method of sample introduction into a gas chromatograph is injection via a microliter syringe into a heated inlet port. The liquid jet from the needle breaks down into particles which evaporate in the carrier gas stream, by interaction with inserts within the inlet port or in contact with the hot inlet port wall. Reproducible rapid vaporization and uniform mixing of the resulting sample vapor with the carrier gas are important for proper separation of the liquid sample components and for determining or minimizing different discrimination errors. Rapid sample vaporization may, however, result in pressure excursions within the inlet port, which can alter the flow-rate through the column [1].

The evaporation rate of the liquid particles produced during an injection depends on their initial size and velocity. The mechanism of liquid jet breakup and particle formation from a sample injector is therefore the first step in the study of inlet port injection performance, and constitutes the subject of this investigation. As it turns out, the size of the particles produced is relatively large and does not lend itself to the commonly perceived flash vaporization process within the carrier gas stream, even at high inlet port temperatures. This leaves interaction with the hot wall or with inserts as the dominant mechanism for vaporization. Additional considerations are that the injection process using a syringe involves plunger motions which are not smooth, resulting in liquid jets with intermittent or variable injection speeds, and that the mechanical motion of the plunger may result in needle tip oscillation producing jets with large lateral motions.

This investigation is the first in a series aimed at examining liquid jet breakup from a commonly used autoinjection system. The specific aims of this work were to record the liquid injection process and to measure the size of particles injected into a simulated inlet port. A needle support system that eliminated large-amplitude lateral motion of the needle tip, and of the emerging liquid jet, allowed conclusions on the ability to generate particles for different fluids and ambient temperatures and on the general requirements for sample vaporization. The sample size used was large (5 μl) to permit a clear identification of the

Correspondence to: Dr. C. E. Polymeropoulos, Department of Mechanical and Aerospace Engineering, Rutgers University, P.O. Box 909, Piscataway, NJ 08855-0909, USA.

* Present address: Graduate Program, Department of Mechanical Engineering, Princeton University, Princeton, NJ 08544, USA.

0021-9673/92/$05.00

different periods during autoinjection. In addition, elevated temperature results were obtained by preheating the gas stream in addition to the wall. Although preheating the gas stream is not part of the chromatographic system under consideration, its use in the present experimentation resulted in a uniform test section environment and permitted easier interpretation of the experimental findings. The majority of the present data were with pure heptane and water as sample liquids to provide variation in surface tension and latent heat of vaporization.

The breakup of a laminar liquid jet issuing from a small orifice has been the subject of numerous experimental and analytical investigations because of its practical importance in the understanding of liquid droplet formation in sprays, in the generation of controlled droplet streams, etc. Several reviews [2,3] can be consulted for treatment of different aspects of the process. Of primary interest has been the amplification of disturbances and drop formation in laminar jets [4–8], jet breakup length [9–11], the influence of ambient and liquid properties and the aerodynamic effect of the surrounding gas [5,8,12–15], etc. Results from these and other previous works will be used as necessary in the discussion of the experimental findings of this work.

EXPERIMENTAL

Fig. 1 is a schematic diagram of the experimental apparatus. The sample injection process employed an autoinjector (Model 7673A automated sampler; Hewlett-Packard) discharging into a heated test section at ambient pressure. Both the test section and the injector were bolted on to a heavy brass plate mounted on a movable platform. A low-speed (18 cm/s), heated air flow was maintained through the test section, which was also equipped with windows for photographic observation of the liquid jet and of the resulting particles. The photographic system employed parallel light from a pulsed (17-ns pulse duration) ruby laser which was triggered via a time delay connected to the control box of the automated injector. The photographic set-up could also be used to record in-line holograms to avoid depth of field problems with measuring small-sized particles at different object distances from the plane of focus. For this work the negatives were evaluated manually using appropriate enlarging optics with a video camera and monitor. Holograms were reconstructed using a helium–neon laser and then evaluated using the same video–monitor system.

Fig. 2 is a more detailed diagram of the test section showing the position of the syringe needle during injection. The needle used was 5 cm × 150 mm I.D. × 650 mm O.D. For the flow-rate and fluids tested, this resulted in fully developed flow at the needle exit. The test section I.D. was 6 cm, and was equipped with two sets of 4 cm wide and 5 cm long quartz windows for photographic observation of the liquid jet and of the resulting particles. The windows were positioned so that one set allowed observation of the liquid in the vicinity of the needle exit, where the jet breakup occurred, and the second set was used for observation of liquid particles to a maximum distance of 15 cm from the needle tip. As shown in Fig. 2, the needle entered the test section through an opening (1 mm in diameter) machined into a 2.5 cm diameter and 3.5 cm long aluminum cylinder attached to the top of the test section. The purpose of this cylinder was to support two rubber

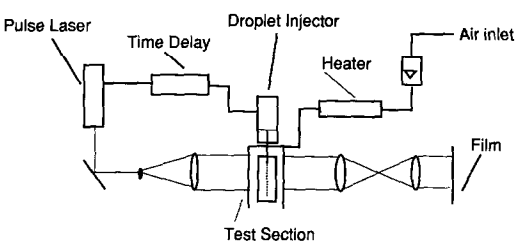

Fig. 1. Schematic diagram of the experimental apparatus.

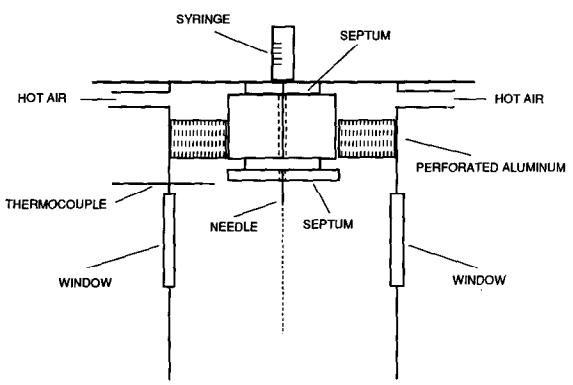

Fig. 2. Test section inlet.

septa 3 mm in diameter and 0.7 mm thick as shown in Fig. 2. The septa sealed the test section entrance, and also provided damping of lateral vibrations of the needle. The needle length was 4 cm and its tip extended 3 mm beyond the second septum.

Air was introduced through the test section using two 4 mm diameter inlet ports and a perforated aluminum plate positioned downstream from the inlets to smooth the gas flow. Two bare thermocouples were used for temperature monitoring and control of the air heater and of the heating tapes which were wrapped around the test section wall. This resulted in almost isothermal conditions within the injection environment. This was verified using a separate movable thermocouple probe with which the maximum temperature difference between any two points within a radius of 2 cm along the test section axis was found to be 2%. The range of temperatures tested was between 20 and 270°C, and the liquids injected were pure heptane and pure water.

Heat transfer from the test section resulted in an increase in the temperature of the syringe and of the fluid inside the sample vial. A separate set of thermocouples were used to check the injector and vial temperatures, which were found to be *ca.* 25°C higher than ambient at the highest test section temperature used. In addition, for the present test conditions, the needle required 100 ms before it reached its final position inside the test section. The combination of higher syringe and fluid temperatures together with the heating of the sample as it passed through the heated syringe during injection will be considered in the interpretation of the experimental results. The liquid speed at the needle exit was calculated from the speed of the syringe plunger, which was recorded on 16-mm film using a high-speed motion picture camera.

RESULTS AND DISCUSSION

Injection periods

Fig. 3 shows the temporal variation of the mean liquid jet speed at the needle exit. For the incompressible liquids used the jet speed was calculated from the measured speed of the syringe plunger motion (also shown in Fig. 3) and the known ratio of plunger to syringe diameter. Fig. 3 shows three distinct periods during the 61-ms injection process,

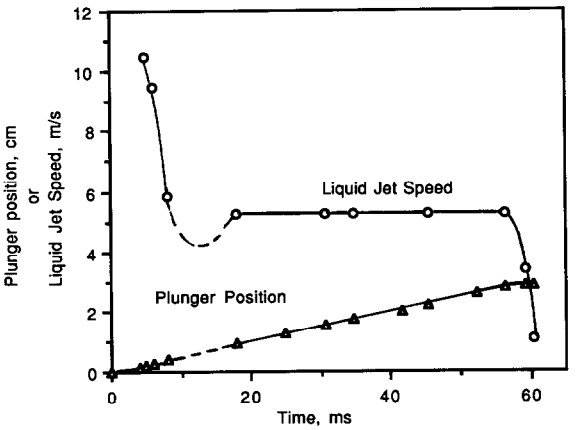

Fig. 3. Syringe plunger position and liquid jet speed during injection.

which are attributed to interactions among the electromechanical components of the injector: (a) an initial unsteady period (0–20 ms) where the jet speed first increased to a maximum of about 10.5 m/s within the first 5 ms and then changed irregularly for the next 15 ms; (b) a steady injection period lasting about 38 ms, where the jet speed was 5.3 m/s; and (c) a final short, *ca.* 3 ms period where the speed dropped to zero as the liquid was depleted. The data for the period between about 10 and 18 ms were insufficient to resolve accurately the shape of the liquid speed curve, and the dashed line was drawn to reflect the observed liquid jet behavior from photography. It should be noted that superimposed on the relatively long time-scale speed variations shown in Fig. 3, the liquid jet was also subjected to small-amplitude, high-frequency disturbances from the injector electromechanical system and from the laboratory environment. These disturbances were amplified resulting in the jet breakup, as will be discussed in the following sections.

Table I gives a summary of the experimental parameters tested and of the steady injection period jet Reynolds and Weber numbers calculated using the steady speed of the jet. The Reynolds numbers at 20°C show that both the water and heptane jets were laminar. At the higher temperature shown (70°C), the Reynolds numbers were near the upper limit of the laminar regime and the jets would be expected to show sensitivity to hydrodynamic disturbances. The Weber numbers for water were sufficiently low for

TABLE I

SUMMARY OF EXPERIMENTAL CONDITIONS

Sample liquids	Water, heptane	
Sample size	5 μl	
Jet diameter, D_j	150 μm	
Injection time	60 ms	
Test section pressure	1 atm	
Test section temperature	20–270°C	
Jet Reynolds number, V_jD_j/ν, at:	20°C	70°C
Water	760	1900
Heptane	1300	2000
Jet Weber number, $\rho D_j^2/\sigma$, at:	20°C	70°C
Water	0.07	0.07
Heptane	0.26	0.26

Rayleigh breakup [2] of the jet, meaning breakup by the growth of axisymmetric oscillatios induced by surface tension. For heptane, the larger Weber numbers place the jet breakup mode within the regime where aerodynamic forces augment the effect of surface tension [2]. The resulting oscillations wavelengths and droplet sizes produced are therefore expected to be smaller for heptane samples [2].

In the following sections, findings related to the initial unsteady and steady-state periods are discussed. The final short, unsteady period at the end of the injection involves a relatively small fraction of the sample and will be examined in future work.

Initial unsteady injection period

Fig. 4a and b show a heptane jet 3 ms after the beginning of injection for 20 and 212°C test section temperatures, respectively. The acceleration of the liquid noted in Fig. 3 resulted in the formation of a large liquid particle at the leading edge of the jet. In addition, during the accelerating period at the beginning of injection, the syringe plunger motion caused intermittent lateral oscillations of the needle tip which show as high-frequency sinuous disturbances on the emerging jet. The speed of the jet leading edge, and of the large particle formed, were around 10 m/s as measured using photographs taken at different times from the beginning of injection.

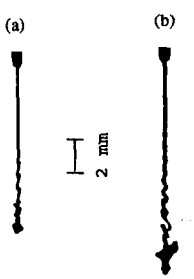

Fig. 4. Heptane jet, initial unsteady period, 3 ms after beginning of injection. (a) 20°C test section temperature; (b) 265°C test section temperature. The needle tip is visible at the top of the photograph.

For the heptane jets in Fig. 4, the leading edge particle (with initial typical major dimension of 1000 μm) had an irregular shape and tended to disintegrate into smaller particles as it travelled downstream. For water jets (not shown), the higher surface tension of water maintained integrity of the large leading edge particle as it travelled through the test section. Particle Weber numbers based on the major particle dimension were *ca.* 6 for heptane and 1.5 for water, and confirm the observed difference in the disintegration process. Additional large particles were also observed during the period between 15 and 20 ms during the irregular motion of the plunger, which is indicated by the dashed line in Fig. 3. The production of such particles was attributed to rapid changes in the jet speed during this period.

The implications of these observations are that the unsteady jet period can produce appreciably sized particles which move at high speeds, *i.e.*, which are not amenable to rapid vaporization, at least within the air stream. Such large particles may also be a significant fraction of the sample size, especially for small injected samples. In such cases rapid vaporization within the inlet port must be accomplished using liquid contact with heated insert surfaces.

Steady injection period

Fig. 5a shows the initial breakup of a water jet in 20°C ambient gas, and Fig. 5b shows the resulting droplets at a mean distance of 12 cm from the needle tip. Fig. 5c and d show similar photographs for a heptane jet. Fig. 5a and c show that the jet breakup was the result of the growth of capillary waves arising from disturbances in the injector environment. The size of the particles produced depended on the wavelength before breakup and both main and satellite droplets were observed. Fig. 5a and c also show evidence of coalescence of droplets after

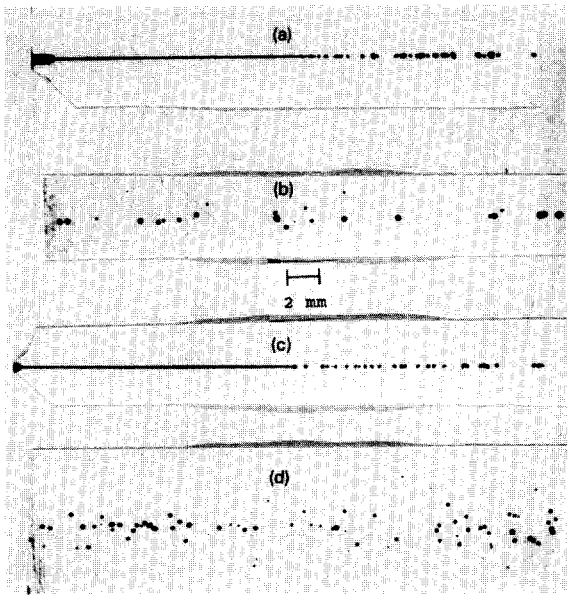

Fig. 5. Steady-state period, 20°C test section temperature. (a) Water jet, 40 ms after the beginning of injection; (b) water particles, 12.5 cm from needle tip, at 50 ms; (c) heptane jet, 50 ms; (d) heptane particles, 12.5 cm from needle tip, 45 ms.

breakup. Fig. 5b and d show that around 12 cm from the needle tip the heptane jet droplets were smaller and showed considerably more radial dispersion than water droplets. The larger droplets from the water jet were due to coalescence between particles moving along the same axis. As is indicated in Fig. 5d, heptane droplets tended to disperse by several millimeters in the radial direction, thus minimizing the probability of coalescence. The magnitude of the observed particle radial dispersion was of the order of the inside radius of typical inlet port inserts. This suggests that during a chromatographic injection significant sample vaporization takes place on the hot insert wall. In addition, lateral oscillations of the needle during injection (such oscillations were mostly suppressed in this work) will promote wall vaporization.

Fig. 6 presents measured mean particle sizes as a function of distance from the needle tip for a 20°C test section temperature. The data are for at least 100 particles per point measured from different photographs taken using the same time delay after the start of injection, and the size of non-spherical

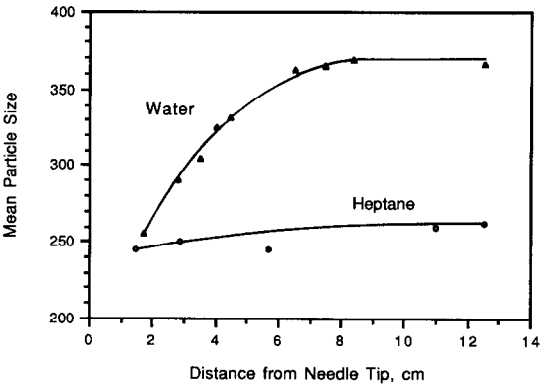

Fig. 6. Variation of arithmetic mean particle size with distance from the needle tip, at 20°C test section temperature. Mean particle size in μm.

particles was recorded as the mean of two major dimensions. For water the coalescence effect shows as a gradual increase in the size of the droplets. There was a very small size increase for heptane particles. Fig. 6 also shows that the mean particle size right after the jet breakup was 256 μm for water. This compares favorably with the value of 260 μm predicted from axisymmetric stability theory at the wavelength of maximum disturbance amplification [16]. For heptane the mean measured particle size near the jet breakup was 245 μm, which is smaller than that for water. The difference is due to the higher jet Weber number for heptane (Table I), which, according to calculations from stability theory, including the aerodynamic influence of the ambient gas [16], yields a slightly shorter wavelength for maximum disturbance amplification.

Fig. 7 shows a typical breakup of a heptane jet for a test section temperature of 265°C. It is noted that the jet surface before breakup was irregular at high temperature and that this resulted in segmentation of the jet. This behavior was typical at elevated test section temperatures and was also observed with water samples. The irregular appearance of the jet

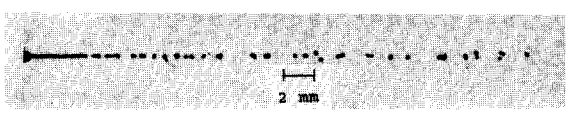

Fig. 7. Heptane jet, at 265°C test section temperature, 40 ms after the beginning of injection.

TABLE II

ESTIMATION OF DROPLET PREHEAT TIME

Liquid	Initial droplet diameter (μm)	Temperature (°C)	Preheat time (ms)
Water	284	265	73
Heptane	278	265	7

surface at elevated test section temperatures is attributed to increased sensitivity of the jet to hydrodynamic disturbances as the jet Reynolds number was increased due heating of the fluid during injection (Table II). Liquid heating during the injection process is influenced by the temperature reached during the initial 100 ms period as the needle enters the heated test section and by the convection process within the syringe as the liquid is pushed out. It is currently difficult to make an accurate prediction of the liquid temperature at the needle exit because of lack of reliable data on the time-varying heat transfer coefficient between the needle outside surface and the hot ambient gas. It is possible, however, to demonstrate that significant heating takes place inside the needle by using a sample fluid of relatively low boiling point and showing that, at a sufficiently high test section temperature, there is evidence of boiling at the needle exit. Fig. 8a and b show a hexane sample

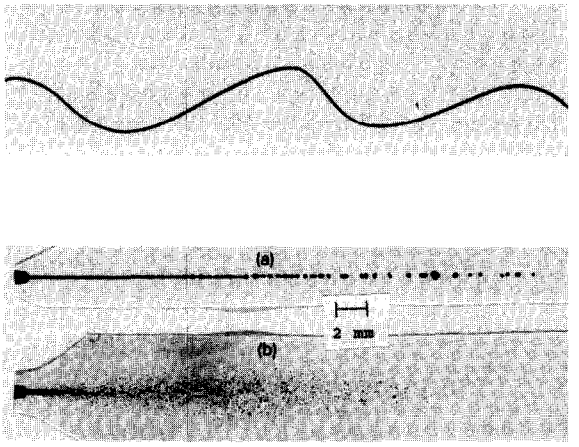

Fig. 8. Hexane jet, 50 ms after the beginning of injection. (a) 20°C test section temperature; (b) 300°C test section temperature.

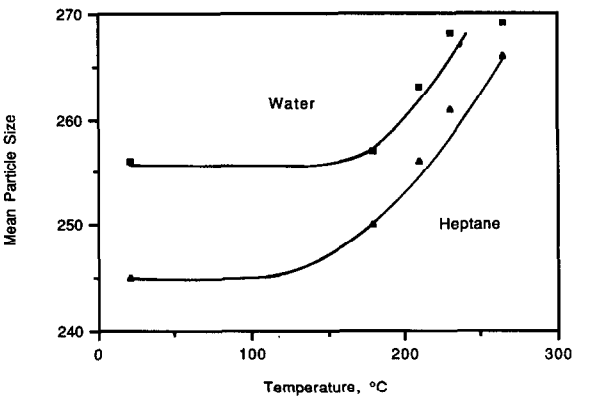

Fig. 9. Variation of the arithmetic mean particle size near the jet breakup with test section temperature. Mean particle size in μm.

injected into the test section at 20 and 300°C, respectively. The large number of small droplets evolving at the needle exit for the high test section temperature is attributed to boiling conditions within the needle. For hexane this means a temperature of at least 68.7°C, which is the normal boiling point of hexane.

The appearance and amplification of irregular disturbances on the jet resulted in jet segmentation, which is evident in Fig. 7. The liquid segments subsequently collapsed into large particles with the net result that the mean particle size after breakup increased as the test section temperature increased. This is indicated in Fig. 9, where the test section

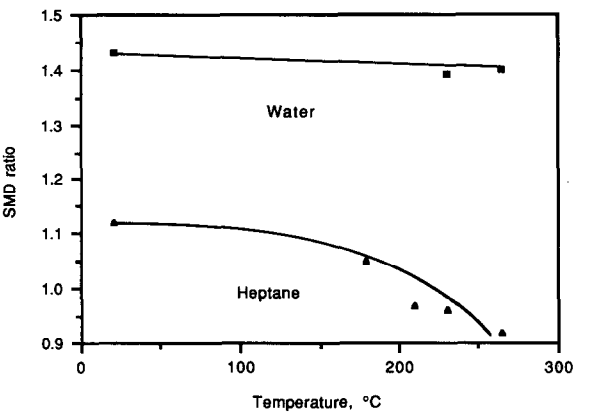

Fig. 10. Ratio of particle Sauter mean diameter at a distance of 12.5 cm from the needle tip to that at jet breakup, as a function of test section temperature.

temperature is plotted against the arithmetic mean particle size for both liquids tested.

The downstream development of particle size at elevated temperatures is suggested by the results in Fig. 10, where the ratio of the Sauter mean diameter 12.5 cm from the needle tip to that after breakup is plotted against the test section temperature (the Sauter [2] mean diameter is used here because it is appropriate for evaporating particles). At low temperatures, this ratio was larger than unity for both samples tested, which is consistent with the results in Fig. 4. As the test section temperature was increased the Sauter mean diameter ratio for water particles increased whereas that for heptane decreased. This is because for the water samples coalescence, which increased the particle size, predominated over the decrease in size due to evaporation. For heptane particles, however, vaporization predominated, resulting in a net decrease in particle size. It is not possible to separate the opposing effects of coalescence and vaporization on particle size. An estimate of incipient vaporization can, however, be furnished by estimating the preheat time, which is the time needed for a water or heptane droplet to reach its equilibrium temperature. This can then be compared with the residence time in the hot environment to estimate the time available for vaporization. Table II shows estimated droplet preheat times calculated using the relationships shown in the Appendix. The preheat times were *ca.* 73 ms for water and only 7 ms for heptane for conditions appropriate to a 265°C test section temperature. The particle residence time travelling at a speed of 5 m/s within the 12.5-cm test section distance is calculated to be *ca.* 24 ms. This shows that the heptane particles were subjected to steady-state vaporization conditions for about 17 ms, whereas water particles did not reach conditions for significant vaporization.

CONCLUSIONS

The breakup of water and heptane liquid jets under conditions encountered with sample autoinjection in a gas chromatograph injection port was examined experimentally using 5-μl samples injected in 61 ms. The specific aims of this work were to measure the size of particles produced with different injection port temperatures in the range 20–270°C and to relate the measurements to conditions relevant to actual sample injections.

It was shown that the motion of the syringe plunger during injection is of primary importance. The initial unsteady (0–20 ms) period of unsteady plunger motion produced large, fast-moving particles which were not subject to rapid vaporization. The subsequent (20–59 ms) steady-state injection period produced particles which conformed to jet breakup stability theory at low test section temperatures. Radial dispersion of the heptane particles was significant, and of the order of a gas chromatographic insert diameter, indicating the importance of liquid vaporization on the insert wall during injection.

At high temperatures, heating of the liquid during injection increased the jet Reynolds number to near the upper limit for laminar jet flow. This resulted in irregular breakup and segmentation of the jet, producing larger particles after the jet as the test section temperature was increased. For heptane samples injected into high test section temperatures, the particle size decreased with distance from the needle tip, while particles from water samples increased in mean size under the same conditions. This was shown to be the result of the competing effects of coalescence and evaporation.

This work is being extended to include examination of various parametric effects, such as sample size, injection speed and sample type, on the particles produced. The work will also includes high-speed motion pictures of the liquid jets and of the particles produced, and a more detailed examination of liquid heating inside the syringe and the needle.

ACKNOWLEDGEMENT

We acknowledge the support of Hewlett-Packard, Avondale Division, for providing equipment necessary for carrying out this work.

APPENDIX

Determination of droplet preheat time

Heat transferred into a liquid droplet which is introduced into a hot environment initially increases the liquid temperature and also contributes to liquid vaporization. Eventually the droplet may reach equilibrium conditions where the temperature remains constant with time and all the heat transferred is used for quasi-steady vaporization. For the relatively large water droplets and ambient conditions

considered, vaporization during the unsteady heat-up period is negligible and calculation of the heat-up time can be carried out using a constant-diameter sphere. Under the assumption of a uniform droplet temperature $T(t)$, an energy balance for a droplet of diameter D initially at temperature T_0 moving inside a hot environment at T_a yields the following relationship for the time, t, to reach different droplet temperatures [17]:

$$t = \frac{\rho C_l}{6K_g(2 + 0.6Re^{0.5})} \cdot D_0^2 \ln\left(\frac{T_a - T_0}{T_a - T}\right) \quad \text{(A1)}$$

where ρ and C_l are the liquid density and specific heat, respectively, K_g is the gas thermal conductivity, $Re = VD/v$ is the droplet Reynolds number based on the droplet speed, V, and v is the kinematic viscosity of the gas. Eqn. A1 is solved for the preheat time, t_s, for which the droplet temperature reaches its equilibrium value, T_s, given by the following equation for quasi-steady vaporization [18]:

$$\frac{Y_s}{1 - Y_s} = \frac{C_g(T_a - T_s)}{L} \quad \text{(A2)}$$

where C_g is the vapor specific heat at constant pressure, L is the latent heat of vaporization and Y_s the equilibrium vapor mass fraction, is given by the Clausius–Clapeyron equation:

$$Y_s = \frac{W_l}{W} \cdot \exp\left[\frac{L}{R}\left(\frac{1}{T_b} - \frac{1}{T_s}\right)\right] \quad \text{(A3)}$$

T_b is the liquid boiling point, W_l is the molecular weight of the liquid and W is the molecular weight of the vapor mixture at the liquid surface.

REFERENCES

1 A. E. Kaufman and C. E. Polymeropoulos, *J. Chromatogr.*, 454 (1988) 23.
2 A. A. Lefebvre, *Atomization and Sprays*, Hemisphere, New York, 1989.
3 L. R. Utreja and D. B. Harmon, American Institute of Aeronautics paper No. 90-1616, Seattle, WA, 1990.
4 W. S. Rayleigh, *Proc. London Math. Soc.*, 4 (1878) 10.
5 E. Goedde and M. C. Yuen, *J. Fluid Mech.*, 40 (1970) 495.
6 A. M. Sterling and C. A. Steicher, *J. Fluid Mech.*, 68 (1975) 477.
7 D. B. Bogy, *Annu. Rev. Fluid Mech.*, 11 (1979) 207.
8 H. Q. Yang, American Institute of Aeronautics paper No. 91-0693, Reno, NV, 1991.
9 R. P. Grant and S. Middleman, *AIChE J.*, 12 (1966) 669.
10 M. J. McCarthy and N. A. Molloy, *Chem. Eng. J.*, 7 (1974) 1.
11 H. Eroglu and N. Chigier, *Phys. Fluids A*, 3 (1990) 303.
12 C. Weber, *Z. Angew. Math. Mech.*, 11 (1931) 136.
13 V. Levich, *Physicochemical Hydrodynamics*, Prentice Hall, Englewood Cliffs, NJ, 1962.
14 R. E. Phiney, *Phys. Fluids*, 16 (1973) 193.
15 R. D. Reitz and F. V. Bracco, *Phys. Fluids*, 22 (1979) 1064.
16 Q. Jun, *M.S. Thesis*, Rutgers University, New Brunswick, NJ, 1991.
17 F. P. Incropera and D. P. De Witt, *Foundations of Heat Transfer*, Wiley, New York, 1990.
18 M. Kanury, *Introduction to Combustion Phenomena*, Gordon & Breach, New York, 1975.